Model Predictive Control based Portable Sulfur Hexafluoride Inflation System

Zhixun Zhang, Minsheng Du, Liang Hua, Binyuan Shi, Dong Lan, Sangen Ding, Binwu Zhang

***Abstract*—Based on the problem that the gas cylinder body is frosted due to the vaporization of liquid SF_6 and absorbs a lot of heat during the inflation of the newly installed GIS equipment and the gas replenishment of the old GIS equipment in engineering applications, the air pressure in the gas cylinder is greatly reduced, and the inflation speed is reduced. It is proposed to design a set of inflation systems that uses temperature compensation to control the inflation rate. To ensure the stable operation of the equipment, the parameters of the temperature compensation device are designed in this paper. Make the system more stable and fast in response. In this paper, the time delay system is simulated and analyzed under the control methods of PID control, Smith control, fuzzy PID control and MPC. Finally, it is concluded that the response speed of the model predictive control method is fast, with strong anti-interference ability. Based on model predictive control, a portable SF_6 inflation system is designed. This design has a one-time investment and obvious economic benefits, which greatly shortens the time and personnel cost of inflation of SF_6 equipment.**

***Index Terms*—SF_6, Smith control, MPC, Time delay system**

I. INTRODUCTION

GIS equipment has high reliability, strong safety, a low maintenance workload, and a maintenance interval for major components of at least 20 years [1-2], contributing significantly to high-voltage, ultra-high voltage, and ultra-high voltage transmission. The primary arc-extinguishing material used in GIS, SF_6 gas, possesses superior arc-extinguishing properties, thermal characteristics, and heat dissipation capabilities, making it particularly suitable for high-voltage and high-current switching operations [3].

To ensure the proper operation of GIS equipment, the working pressure of SF_6 gas is typically maintained at 0.5 MPa (gauge pressure). If the pressure drops to 0.4 MPa (gauge pressure), a low-pressure alarm is triggered, necessitating prompt gas replenishment [4]. Low-voltage alarms can arise from two causes. The failure is primarily caused by aging GIS equipment, which leads to porosity in hard sealing materials, cracks in the welding of copper pipes, defects in the manufacturing of sealing gaskets, and poor finish of the globe valve [5]. As a result, the equipment leakage rate is approximately 2% to 4% of the equipment volume annually [6]. Non-fault cause: Leakage of SF_6 gas within the normal range, the SF_6 gas leakage rate is less than 1% in the Preventive Experimental Regulations for Electric Power Equipment, the Regulations and Technical Indicators for Equipment Condition Maintenance of the State Grid Corporation of China, and the Guidelines for Gas Management and Detection in Sulfur Hexafluoride Electrical Equipment [7]. SF_6 gas decomposes under arc, corona, and partial discharge conditions [8-9]. Whether newly installed GIS equipment in power grid construction or older GIS equipment with abnormal air pressure, SF_6 gas supplementation is required. Therefore, efficient and safe SF_6 inflation equipment is crucial for both power grid construction and the stable operation of the power system.

In the process of gas direct charging of GIS equipment, the bottled liquid SF_6 vaporization process cannot quantify the characteristic relationship between gas temperature, pressure and flow rate, and the "critical point" of the three cannot be determined, resulting in the reduction of cylinder temperature and frost in the filling process, and the insufficient vaporization of some liquid SF_6 gases causes waste. Existing SF_6 gas inflation technologies, both domestically and internationally, are mainly classified into two categories. One is manual control, which utilizes a mobile platform or portable cart with a gas cylinder heating device to compensate for the temperature drop during SF_6 vaporization, thereby increasing cylinder pressure and improving inflation efficiency. The second is the semi-automatic inflation method, which uses a PLC-controlled SF_6 automatic inflator with a gas pressure sensor to regulate gas chamber pressure and control the solenoid valve for automatic gas inflation. The manual control method requires monitoring the readings of the pressure-reducing valve and two pressure gauges to assess inflation status and determine whether the inflation amount meets standards. At the end of inflation, the pressure control accuracy is often poor. The semi-automatic method lacks a cylinder temperature compensation device, resulting in prolonged inflation times and reduced inflation efficiency.

Aiming at the problems of insufficient vaporization of liquid SF_6 in the process of inflation, resulting in waste, poor

Manuscript received May 29, 2024; revised February 05, 2025.
Zhixun Zhang is an engineer at Gansu Power Transmission and Transformation Co.Ltd., LZ 730000 China (corresponding author to provide phone: 0086-931-2363622; fax: 0086-931-2363622; e-mail: zhangxsir@yeah.net).
Minsheng Du is a deputy senior engineer at Gansu Power Transmission and Transformation Co., Ltd., LZ 730000 China. (e-mail: duminsheng@163.com).
Liang Hua is a deputy senior engineer at Gansu Power Transmission and Transformation Co.Ltd., LZ 730000 China. (e-mail: hualiang@163.com).
Binyuan Shi is a deputy senior engineer at Gansu Power Transmission and Transformation Co.Ltd., LZ 730000 China. (e-mail: shibinyuan@163.com).
Dong Lan is a deputy senior engineer at Gansu Power Transmission and Transformation Co.Ltd., LZ 730000 China. (e-mail: landong@163.com).
Sangen Ding is an engineer at Gansu Power Transmission and Transformation Co.Ltd., LZ 730000 China. (e-mail: dingsangen@163.com).
Binwu Zhang is an engineer at State Grid Wuwei Power Supply Company Co.Ltd., WW 733000 China. (e-mail: zhangbinwu@163.com).

pressure control accuracy, and non-standard inflation. This paper proposes a portable SF_6 inflation system based on model predictive control. By mathematically modeling pressure changes in the SF_6 cylinder during heating, a transfer function is derived. Various control methods are then applied to simulate the heating process, evaluating the accuracy and stability of each control mode to design the most accurate and stable control system. By incorporating weighing, temperature measurement, pressure detection, electronic pressure-reducing valves, and other components, the system aims to precisely control pressure, temperature, flow, and inflation. This will reduce labor costs, minimize resource waste, and ensure the safe and stable operation of electrical equipment, as well as the safety of construction personnel.

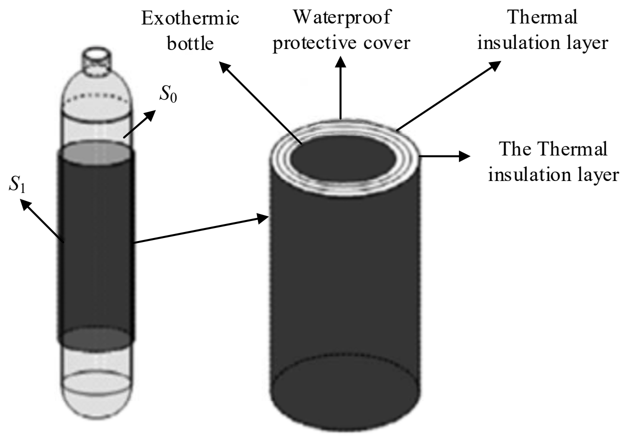

Fig. 1. Structure diagram of Heating and insulation device

II. Establishment Of Inflatable Models

A. Heating Insulation Device Design

The critical temperature of SF_6 is 318.72 K, and its critical pressure is 3.733 MPa. At low temperatures and high pressures, the molecular interactions become significant, leading to an increase in gas density and intermolecular forces. As a result, molecular volume and intermolecular forces cannot be neglected, and the ideal gas law is no longer applicable [10]. In this paper, the state parameters of SF_6 were calculated using the Beattie-Bridgman empirical formula, while the saturated vapor pressure curve of SF_6 gas, as studied by Pan Ruiqiong et al. [11], was used to determine the saturated vapor pressure at various temperatures. Additional SF_6 parameters were obtained from the NIST Refprop database.

As shown in Fig. 1, the equivalent heat dissipation area corresponds to the equivalent heat source area. The heating insulation device consists of an electric heating board, a thermal insulation layer, and a waterproof protective sleeve, ensuring high work efficiency, long service life, and versatility in use. The SF_6 cylinder has a diameter of 220 mm, a height of 1450 mm, and a filling coefficient of 1.17 kg/L at room temperature, with an operating pressure range of 2.1 to 2.3 MPa. The corresponding surface area is 449,020 mm² and 552,640 mm².

Based on the actual heat transfer characteristics of the SF_6 cylinder deflation process, as illustrated in Fig. 2, this paper constructs the gas and the bottle wall, the heat conduction between the inside and outside sides of the bottle wall, the heat exchange between the bottle wall and the external environment, the SF_6 liquid vaporization and heat absorption, and the thermal radiation of the outer wall of the cylinder facing the air [12- 15], and the detailed modeling methods are as follows. When the pressure-reducing valve is opened, the heat transfer rate between the SF_6 gas and the inner wall surface is calculated as follows:

$$\delta Q_i = h_i A_i (T_i - T) \tag{1}$$

Type: δQ_i is the convective heat transfer heat flow of SF_6 gas, W; h_i is the heat transfer coefficient of the flow on the inner wall of the cylinder, $\mathrm{W/(m^2 \cdot K)}$; A_i is the heat exchange area of the inner wall of the cylinder, m^2 ; T_i is the heat exchange temperature of the inner wall of the cylinder, K.

During the deflation process, the heat transfer mode between the gas and the inner wall is forced convective heat transfer, and the formula for calculating the convective heat transfer coefficient is as follows:

$$h_i = 0.023 \times \mathrm{Re}^{0.8} \times \mathrm{Pr}^{0.4} \times \frac{l_{He}}{L} \tag{2}$$

Type: Re is the Reynolds number of a gas, dimensionless; Pr is the Prandtl number of a gas, dimensionless; l_{He} is gas thermal conductivity, $\mathrm{W/(m \cdot k)}$; L is the characteristic scale, m.

The formula for calculating the radial thermal conduction heat flow between the inner and outer walls of a gas cylinder is as follows:

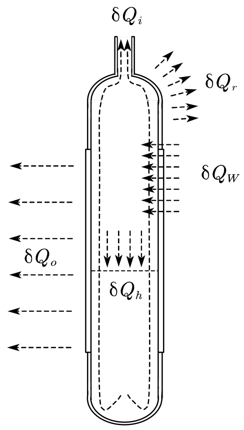

Fig. 2. Schematic diagram of SF_6 cylinder heat transfer during deflating process

$$\delta Q_w = \frac{4\pi\lambda_w (T_o - T_i)}{1/r_i - 1/r_o} \tag{3}$$

Type: δQ_w is the heat flow of heat conduction on the cylinder wall, W; λ_w is the thermal conductivity of the gas cylinder wall, $\mathrm{W/(m \cdot k)}$; T_O and T_i are the temperature of the outer and inner walls of the cylinder, K; r_o and r_i are the radius of the outer and inner walls of the gas cylinder, m.

The formula for calculating the convective heat transfer between the outer wall of the cylinder and the air is as follows:

$$\delta Q_o = h_o A_o (T_{Air} - T_o) \quad (4)$$

Type: δQ_o is the heat flow of heat exchange on the outer wall of the cylinder, W; h_o is the convective heat transfer coefficient of the cylinder outer wall, $\mathrm{W/(m^2 \cdot K)}$; A_o is the heat exchange area on the outer wall of the gas cylinder, $\mathrm{m^2}$; T_{Air} is the air temperature outside the cylinder, K.

The heat transfer between the outer wall and the air is usually natural convection. When the wind speed is taken into account, the calculation should follow the formula provided in equation (5). In the absence of wind, the convective heat transfer coefficient is determined using the natural convection heat transfer formula:

$$h_o = 0.27 \times (\mathrm{Gr} \times \mathrm{Pr})^{0.25} \times \frac{\lambda}{L} \quad (5)$$

Typ: Gr is Grachov a number of gaseous medium, dimensionless; λ is the thermal conductivity of air, $\mathrm{W/(m \cdot k)}$.

The thermal radiation between the outer wall of the cylinder and the air can be calculated by the following formula:

$$\delta Q_r = A_r \times \varepsilon \times \sigma \times (T_{Air}^4 - T_o^4) \quad (6)$$

Type: ε is the emission amount of matter; σ is Steppan-Boltzmann constant.

Fig. 2 δQ_h illustrates the latent heat of vaporization absorbed when liquid SF_6 is vaporized into SF_6 gas. Within a specified error range, the mass of gas released in the gas-liquid equilibrium state within the cylinder at a constant temperature can be approximated as the mass of liquid SF_6 converted into gaseous SF_6.

To ensure the equipment operates effectively in low-temperature environments, the minimum temperature is based on the lowest recorded temperature of 242K in Gansu Province over the past 50 years. To increase the inflation rate, the supplementary temperature is raised to 27K. At this point, the air pressure in the cylinder reaches 1.118 MPa, which is 0.5 MPa higher than the rated air pressure of typical GIS equipment (0.6 MPa) to ensure the inflation rate is achieved.

When the pressure-reducing valve is opened, the gas temperature is the same as the cylinder temperature. To ensure the external heating device has sufficient power, the temperature difference is assumed to be 1K. Forced convection coefficient h_i=163.334 $\mathrm{W/(m^2 \cdot K)}$, change the flow area of A_t=0.945 $\mathrm{m^2}$, temperature difference ΔT_i=1K, Gas convection heat transfer heat flow δQ_o=154W.

The thermal conductivity of radial thermal cylinder λ_w=60 $\mathrm{W/(m \cdot k)}$, the temperature difference between inner and outer walls of cylinder ΔT=1K, the cylinder outer wall radius r_o=0.110m, the cylinder inner wall radius r_i=0.104m. Substituting these value into Equation (3) to obtain the heat flow of cylinder wall conduction δQ_w=1437W.

The natural convection coefficient, in the absence of wind, is $h_o^{'}$=5.814 $\mathrm{W/(m^2 \cdot K)}$, with a temperature difference of ΔT_A=27K, and the natural convection heat transfer of air is $\delta Q_o^{'}$=148W. From November to February in Gansu Province from 1971 to 2000, the anemometer took the highest wind speed of 4M /s for calculation, and the forced convection system $h_o^{''}$=105.467 $\mathrm{W/(m^2 \cdot K)}$, air forced convection heat transfer heat flow $\delta Q_o^{''}$=2690W. The total air convection heat transfer heat flow $\delta Q_o = \delta Q_o^{'} + \delta Q_o^{''}$=2838W. According to the design, the flow rate of SF_6 gas is approximately 0.01kg/s. Based on Table I, the latent heat of vaporization of liquid SF_6 at 269 K was calculated to be δQ_h=862W.

TABLE I
LATENT HEAT OF SF_6 VAPORIZATION AT DIFFERENT TEMPERATURES

Tem-Pera-ture K	Vapori-zation Latent heat of kJ/kg	Tem-Pera-ture K	Vapori-zation Latent heat of kJ/kg	Tem-Pera-ture K	Vapori-zation Latent heat of kJ/kg
243	101.735	263	90.667	283	76.303
248	99.191	268	87.459	288	71.904
253	96.510	273	84.022	293	67.024
258	93.675	278	80.319	298	61.512

Emission of thermal radiation material from the outer wall the of gas cylinder and air ε=0.9, the Steppan-boltzmann constant σ=5.67×10^{-8}, and the radiating area A_r=1.097 $\mathrm{m^2}$. The heat transfer from the outer wall of the cylinder to the air is δQ_r=101W.

The power of the gas cylinder heating insulation device is: $Q = \delta Q_i + \delta Q_w + \delta Q_o + \delta Q_h + \delta Q_r$=5383W.

B. Mathematical model of cylinder deflation

In the actual inflation process, the primary factor influencing inflation is the heat absorption during the vaporization of liquid SF_6, which causes a rapid temperature drop in the cylinder and a corresponding decrease in air pressure and inflation speed. In this paper, under the condition of 250K ambient temperature and wind speed 2m/s, an organic analysis method is employed to establish the mathematical model for gas cylinder operation. The organic analysis method reveals the relationship between internal system variables and system performance, and establishes a mathematical model where the input and output variables of the controlled system are met [16].

When heated, the amount of heat absorbed by gaseous SF_6 is:

$$W_1 = C_g \times \rho_g \times V_g \times \Delta T_1 \tag{7}$$

The heat absorption of latent heat of vaporization during exhaust is:

$$W_2 = Q_h \times Q_m \times T_1 \times \Delta_t \tag{8}$$

The heat lost from the cylinder is:

$$W_3 = k \times \Delta T_1 \tag{9}$$

The heat absorbed by the cylinder is:

$$W_4 = C_s \times m_s \times \Delta T_1 \tag{10}$$

When heated, the heat absorbed by liquid SF_6 is:

$$W_5 = C_l \times \rho_l \times V_l \times \Delta T_1 \tag{11}$$

Total heat generated by the heating and insulation device:

$$W = u \times W_m \times \Delta_t \tag{12}$$

According to the energy conservation relation, the following can be obtained:

$$W = W_1 + W_2 + W_3 + W_4 + W_5 \tag{13}$$

Substitute equations (7-12) into Equation (13) and simplify to:

$$T_p \times \frac{\Delta T_1}{\Delta_t} + T_1 = K_P \times u \tag{14}$$

In the type:

$$T_p = \frac{C_g \rho_g V_g + k + C_s m_s + C_l \rho_l (V - V_g)}{Q_h Q_m} \tag{15}$$

$$K_P = \frac{W_m}{Q_h Q_m} \tag{16}$$

Taking the Laplace transform of Equation (14), the expression is:

$$\frac{T_1(s)}{u(s)} = \frac{K_p}{T_p s + 1} \tag{17}$$

The electric heating device is a self-balancing system, which can be represented by a pure lag link of a second-order system. This second-order system can be simplified to a first-order model through parameter identification. Thus, the first-order inertia lag link can be used to represent the mathematical model of the system [17-19]. Its transfer function is as follows:

$$G(s) = \frac{K}{Ts + 1} e^{-\tau s} \tag{18}$$

Mathematical modeling was conducted based on the relationships between physical quantities established by the organic analysis method described above. The following assumptions were made during the modeling process: 1: The gaseous and liquid sulfur hexafluoride in the cylinder are regarded as isotherms; 2: The cylinder discharges at a constant flow rate; 3: The sulfur hexafluoride change process in the cylinder is considered to occur at constant volume, with the heat absorbed by temperature change treated as the constant volume specific heat capacity. By solving for the temperature, the temperature variations under different heating powers can be obtained. The temperature variations at 3000W are presented in Fig. 3.

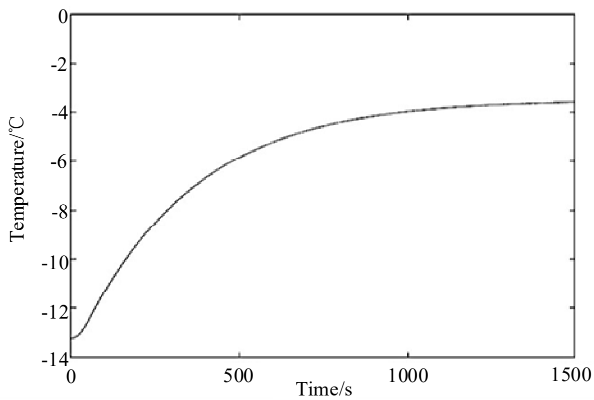

Fig. 3. Temperature variation of sulfur hexafluoride at 3000w power

According to the calculation method [20], the transfer function of the first-order inertia lag link is obtained, and the proportional gain K is obtained by using the formula (19). Two points on the temperature curve are obtained by using the formula (20-23) T, τ .

$$K = \frac{y(\infty) - y(0)}{\Delta u} \tag{19}$$

$$y^*(t) = \frac{y(t)}{y(\infty)} \tag{20}$$

$$y^*(t) = \begin{cases} 0 & t < \tau \\ 1 - \exp(-\frac{t-\tau}{T}) & t > \tau \end{cases} \tag{21}$$

$$\begin{cases} y^*(t_1) = 1 - exp(-\frac{t_1 - \tau}{T}) \\ y^*(t_2) = 1 - exp(-\frac{t_2 - \tau}{T}) \end{cases} \tag{22}$$

$$\begin{cases} T = \dfrac{t_2 - t_1}{ln\left[1-y^*(t_1)\right]-ln\left[1-y^*(t_2)\right]} \\ t = \dfrac{t_2 ln\left[1-y^*(t_1)\right]-t_1 ln\left[1-y^*(t_2)\right]}{ln\left[1-y^*(t_1)\right]-ln\left[1-y^*(t_2)\right]} \end{cases} \tag{23}$$

$$\begin{cases} T = 2(t_2 - t_1) \\ t = 2t_1 - t_2 \end{cases} \tag{24}$$

$$G(s) = \frac{0.58}{320s+1}e^{-26s} \tag{25}$$

III. INFLATABLE SYSTEM DESIGN

A. Hardware design of inflation system

The inflation system automates the inflation process by controlling the decompression solenoid valve and the heating device. The system consists of three parts: data acquisition, microprocessor control and actuator. The data acquisition is to collect the data obtained from the pressure detection module, flow detection module, temperature detection module, and weight detection module. The actuator is made of the heating device module and the charging and discharging solenoid valve module by the microprocessor. System hardware composition is shown in Fig. 4.

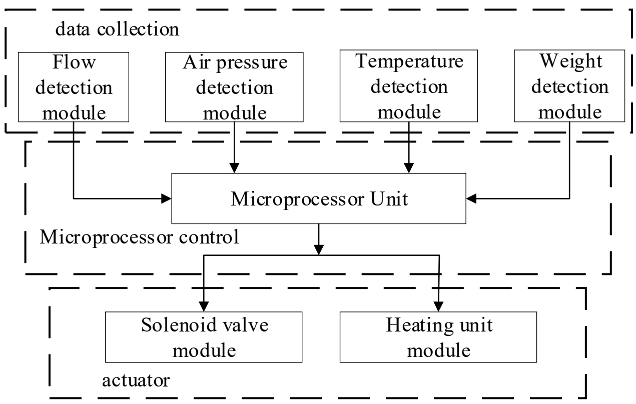

Fig. 4. Hardware diagram of inflation system

The system flow module selects the ALICAT 21 series standard mass flow controller with fast response and strong stability. The heating device choice of long life, and resistance to dry burning stainless steel electric heating tube. The temperature detection module uses the DS18B20 temperature sensor, which offers a wide temperature measurement range and high collision resistance. The pressure detection module selects of large range, high precision hard film pressure transmitter.

B. Inflatable system software design

During the filling process, the external temperature of the cylinder, the weight of both the cylinder and internal SF_6, the cylinder pressure, and the GIS equipment pressure are measured by sensors. The processor inputs the measured temperature and pressure into the Beattie-Bridgman empirical formula for calculation and determines the current GIS gas density. By comparing this with the gas density at rated temperature and pressure, the required supplementary gas mass is calculated. The data from the weight sensor is used to verify whether the weight of the remaining gas in the cylinder meets the filling requirements. By substituting the pressure and pressure in the cylinder into the formula in paper [11], the current cylinder temperature can be confirmed to determine whether heating is needed. T The inflated mass is determined using both the flow sensor and the weight sensor to enhance system reliability. The specific action flow of the inflation system is shown in Fig. 5.

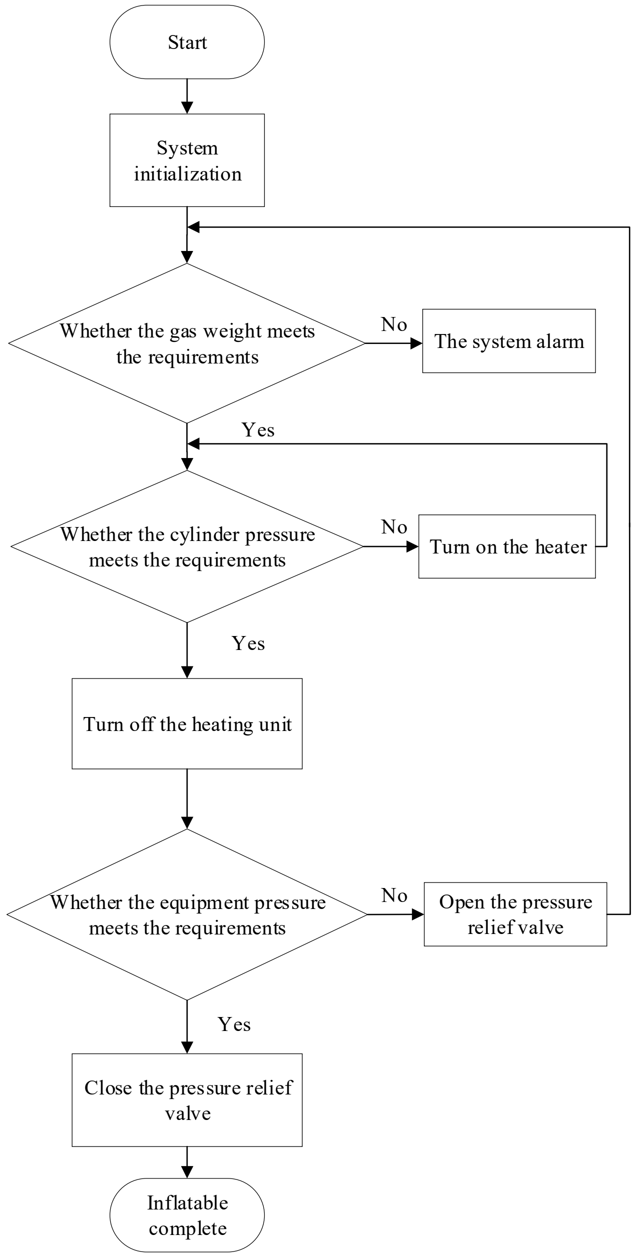

Fig. 5. Action flow chart of inflatable system

IV. INFLATION CONTROL STRATEGY

A. Control Principles

The inflatable system of GIS equipment primarily operates in an open outdoor environment, where wind speeds and ambient temperature can significantly disturb the system. Due to the wide variation in wind speeds and temperatures in the environment, the system must possess strong interference suppression capabilities. According to Equation (27), the inflatable system can be modeled as a first-order inertia hysteresis system. Due to the relationship between pure hysteresis time and the system's process time constant (T), conventional control methods cannot provide timely feedback, leading to increased system overshoot, slow and prolonged adjustment time, and the system will also appear shock and instability.

To ensure that the inflation system exhibits good stability, strong anti-interference capability, fast response speed, and minimal overshoot, this paper applies the Ziegler-Nichols method to adjust the parameters of the traditional PID control. It is modified on the basis of PID to add differential first control and intermediate differential control, so as to suppress the overshoot of the hysteresis system and reduce the system adjustment time [21]. The block diagram of the differential first control is shown in Fig. 6, and the block diagram of the intermediate differential feedback control is shown in Fig. 7.

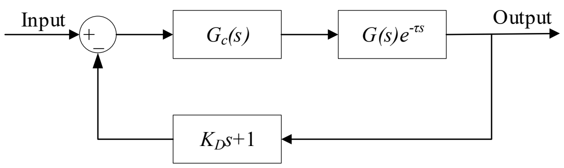

Fig. 6. Differential first control block diagram

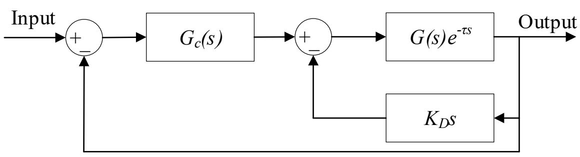

Fig. 7. Block diagram of intermediate differential feedback control

The traditional PID control method has strong traceability but weak disturbance rejection ability. To address this issue, this paper combines traditional PID control with fuzzy control. Fuzzy PID control can effectively adjust the control parameters, possess logical reasoning capability, and improve disturbance rejection. The block diagram of the fuzzy PID control is shown in Fig. 8.

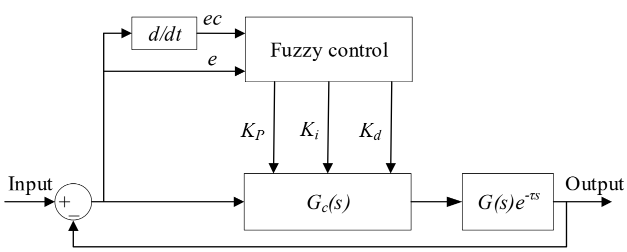

Fig. 8. Fuzzy PID control block diagram

Pure lag time lag system link influences the zero pole distribution system, in which the output signal does not timely feedback, the control effect is poor, based on the Smith prediction control transfers lag link to the outside of the closed-loop system to make it without lag part of the characteristic equation, combined with PID control, increase the control effect, Smith prediction control block diagram as shown in Fig. 9.

In this paper, a regulator is incorporated into Smith predictive control to reduce its sensitivity to model accuracy requirements, thereby improving the control performance of the system. The block diagram of improved Smith predictive control is shown in Fig. 10.

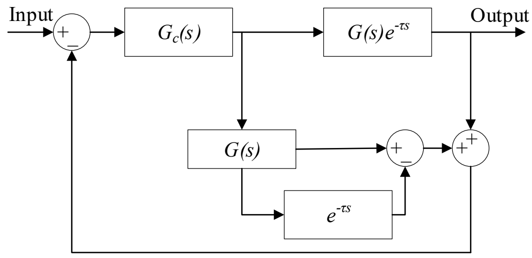

Fig. 9. Smith predictive control block diagram

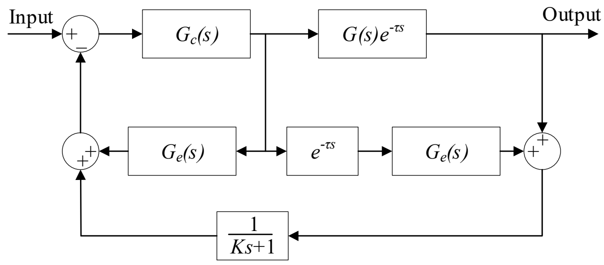

Fig. 10. Improved smith predictive control

In this paper, the pneumatic system of a specific task is accurately modeled to account for environmental changes and external factors, which can be considered as interference. Based on the proposed model, model predictive control is employed to simulate the output prediction, feedback correction, and rolling optimization. The block diagram of the model predictive control system is shown in Fig. 11.

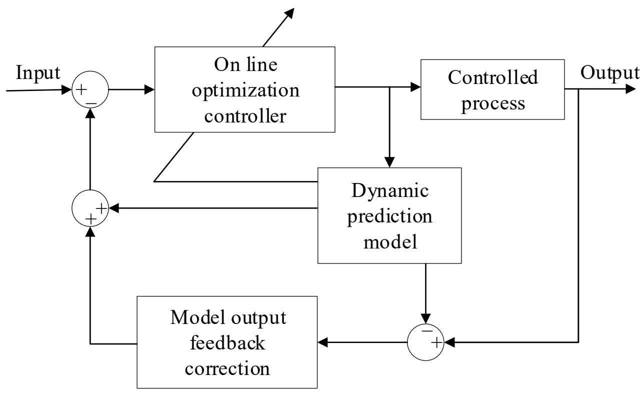

Fig. 11. Model predictive control block diagram

The proposed method addresses the existing issues of the system to some extent. This paper compares the aforementioned methods for modeling and controlling interference.

B. *Analysis of control results*

In PID control, the P parameter is set to 4, the I parameter is set to 0.055, and the D parameter is set to 0.0132. In the differential preemptive control, the P parameter is set to 5, and other parameters remain consistent with those of the PID control.

The parameters of the intermediate differential control are consistent with those of the differential antecedent control. In Smith's control, the P parameter is set to 16, and the improved k is set to 2. The fuzzy PID control inputs are the error and the error change rate, which constitute a 2-input, 3-output fuzzy controller with 49 rules. The input quantization factor of E is set to 3.03, the EC quantization factor is set to 1, and the output proportional factors of the PID are set to 1, 0.97, and 1.15, respectively.

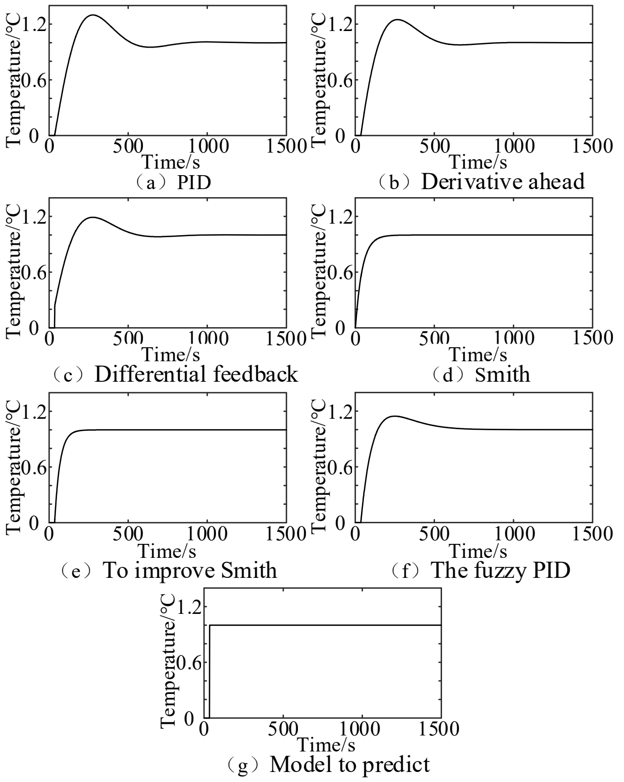

Fig. 12. Rendering of the inflatable system response

The model input is a step function with a step size of 1, and the system response is compared in terms of overshoot, adjustment time, and rise time. The adjustment time is defined as the time required to reach 5% of the steady-state value. The system's response is shown in Fig. 12, and the simulation results are compared in Table II.

TABLE II
COMPARISON OF SIMULATION RESULTS OF DIFFERENT CONTROL STRATEGIES

Control scheme	Overshoot amount /%	Adjust the time /s	Rise time /s
Conventional PID	34.4%	672s	92s
Derivative ahead	27.7%	414s	85s
Differential feedback	22.3%	425s	99s
Smith	0.4%	98s	75s
To improve the Smith	0%	118s	68s
The fuzzy PID	18.2%	478s	75s
Model to predict	0.2%	30s	3s

It can be clearly seen from Table II that the model predictive control has a small overshoot, short adjustment time and rise time, and its response speed far exceeds other control methods. For the inflatable system operating in different environments, it is equivalent to adding interference to the system. In this paper, an interference signal with an amplitude of 0.2 is introduced when the 1100S system reaches a stable state.

The system's response to interference is depicted in Fig. 13, with the corresponding data presented in Table III. It can be seen from the table that the model predictive control restores stability in a very short time and demonstrates excellent anti-interference capabilities. Based on the data above, it can be concluded that model predictive control offers fast response speed, small overshoot, robust anti-interference capability, and meets the system’s design requirements.

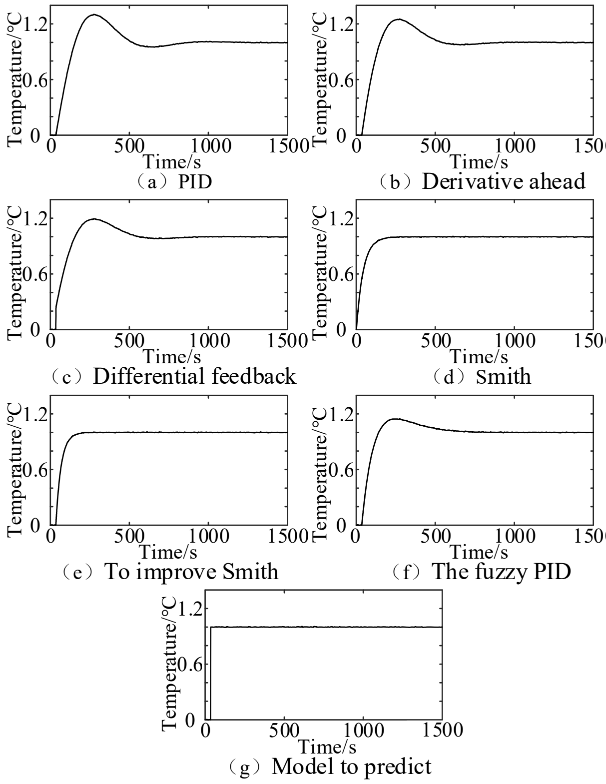

Fig. 13. Effect drawing of inflatable system response under disturbance

TABLE III
COMPARISON OF SIMULATION RESULTS UNDER DIFFERENT CONTROL STRATEGIES

Control scheme	breadth /%	Shock time /s	Immunity characteristic
Conventional PID	9.5%	340s	poor
Derivative ahead	10.5%	342s	poor
Differential feedback	10.5%	341s	poor
Smith	4.5%	100s	good
To improve the Smith	8.5%	103s	general
The fuzzy PID	9.5%	237s	general
Model to predict	3.0%	54s	Very good

V. CONCLUSION

This paper explains the SF_6 loss in current GIS equipment and the role of SF_6 under rated air pressure. It also describes the importance of air filling and inflation, as well as the main challenges currently faced. First, a heat conduction mathematical model of the SF_6 inflation process is developed, based on the physical properties of SF_6 gas and the structure and parameters of the gas cylinder. A mathematical model of the cylinder deflation process is also established using organic analysis. Second, the hardware and software control of the portable SF_6 automatic inflation system, which regulates the inflation rate through temperature compensation, are designed based on the mathematical model of the cylinder deflation process. Finally, the automatic filling system is simulated and analyzed using PID control, Smith control, fuzzy PID control, and MPC control strategies. The results show that the model predicts fast response, small overshoot, and strong anti-interference, meeting the system's design requirements. Additionally, cost estimation for the system's operation shows that this design is a one-time investment with clear economic benefits. It significantly reduces SF_6 equipment inflation time and personnel costs. With five people working 8 hours per day and a labor cost of 100 yuan per hour per person, the system saves 4,000 yuan per day. In the conventional inflation mode, it takes about 60 days for the 330 kV GIS equipment substation, while the new system reduces this to about 30 days, yielding a direct economic benefit of approximately 400,000 yuan. Indirect economic benefits include energy savings and emission reductions. This result significantly reduces gas waste and damage, improving material utilization. Finally, the design of the research while solving the current equipment of the main problems in the air, but only for a single cylinder were analyzed, and the GIS equipment in the substation equipment needed for gas often single cylinder can't meet, still need to analyze the multiple cylinders combined aeration system design to meet the requirements of large capacity equipment inflatable, need further exploration and research.

REFERENCES

[1] Fei Chen, "Research on development and application of GIS equipment," M.S. thesis, Dept. Elect. Eng., Zhejiang Univ., Zhejiang Province, China, 2007.

[2] Dan Zhang, Haisong Xu, and Dingqian Yang, "Study on the aging characteristics of PET for SF_6 gas-insulated transformer," *AIP Advances*, vo l. 14, no. 7, 2024.

[3] Ziyuan Zhao, Enyuan Dong, and Yifei Zhang, "Influence of SF_6/N_2 Mixed Gas Pressure on the Arc Control Ability of the Main Electrode in the Trigger Gap," *Journal of Physics: Conference Series*, vol. 2800, no. 1, 2024.

[4] Yue Yang, "Analysis on the infrared imaging technology in the leak detection of SF_6 charged equipment," M.S. thesis, Dept. Elect. Eng., North China Electric Power Univ., Hebei Province, China, 2014.

[5] Guoguang Zhang, *Live testing technology and fault diagnosis of electrical power unit*. Beijing: China Electric Power Press, pp. 176-181, 2015.

[6] Yongxiang Li, Tianzheng Wang, and Yanpeng Li, "Abnormal Analysis of GIS Electrical Equipment Gas Leakage Based on Infrared Imaging Leakage Detection Technology," *High Voltage Apparatus*, vol. 52, no. 7, pp. 185-191, 2016.

[7] *The guide for management and measuring SF_6 gas in electrical equipment*, GB/T 8905-2012, 2012.

[8] Youwei Liu, Liyuan Wu, and Yanpeng Gong, "Investigation on SF_6 Decomposition Products in GIS and Affecting Factors," *Power System Technology*, vol. 33, no. 5, pp. 58-61, 2009.

[9] Yu Wang, Zhi Li, and Weijian Yao, "Analysis of SF_6 Byproducts of Gas Insulated Switchgear in Guangdong Province," *High Voltage Engineering*, vol. 35, no. 4, pp. 823-827, 2009.

[10] Xiaomin Zhao, Guohui Han, and Wenkui Liu, "Liquefaction and State Parameters of SF_6/CF_4 Mixed Gas in High Voltage Circuit Breaker," *High Voltage Apparatus*, vol. 52, no. 12, pp. 204-208, 2016.

[11] Ruiqiong Pan and Wenyong Wang, "Approximation Formula and Application of SF_6 Saturated Steam Pressure Curve," *High Voltage Apparatus*, no. 2, pp. 155-156, 2006.

[12] Kai Wang, Erfeng Chen, and Yi Zhang, "Simulation and Experimental Validation on Charge/Discharge of Composite Cylinders," *Pressure Vessel Technology*, vol. 33, no. 12, pp. 1-6, 2016.

[13] S. W. Churchill and H. H. S. Chu, "Correlating equations for laminar and trubulent free convection from a vertical plate," *Int J Heat Mass Transfer*, vol. 18, no. 9, pp. 1024, 1975.

[14] Jingzhou Zhang, Haiping Chang, and Xiaoming Tan, *Heat transfer Heat transfer*. Beijing: Science Press, pp. 52-55, 2019.

[15] Shiyan Pan and Qing Yuan, "Heating Calculation of SF_6 Combined Electric Appliance in the Alpine Region," *Journal of Shanghai Electric Technology*, vol. 5, no. 4, pp.1-3, 2012.

[16] Qingkun Yu, Jixin Ding, and Libing Wu, "Event-Triggered Prescribed Time Adaptive Fuzzy Fault-Tolerant Control for Nonlinear Systems With Full-State Constraints," *Engineering Letters*, vol. 32, no. 8, pp. 1577-1584, 2024.

[17] Qiang Li, "The Study of Delay Temprature System Control," M.S. thesis, Dept. Elect. Eng., Southwest Jiaotong Univ., Sichuan Province, China, 2009.

[18] Jianjun Liu, "The Implementation and Optimization of Control Algorithm for Large Time Delay System Over Heating Water Tank Based on PLC," M.S. thesise, Dept. of Auto., Inner Moncolia Univ. Inner Mongolia Autonomous Region, China, 2016.

[19] Kai Ren and Leren Tao, "Simulation Study on Suction Vapor Quality Control of Compressor Based on Fuzzy PID," *Modeling and Simulation*, vol. 12, no. 4, pp. 3684-3696, 2023.

[20] Zhenglin Wang, *Process Control Engineering and Simulation: Based on MATLAB/Simulin*. Beijing: Publishing House of Electronics Industry, pp. 132-139, 2009.

[21] Dingyu Xue, *Control System Simulation and Computer Aided Design*. Beijing: China Machine Press, pp. 340-358, 2009.

Zhixun Zhang The corresponding author. He main research directions are the design of improved Smith predictor controllers, the development of smart grid technology and management change. He is an engineer at Gansu Power Transmission and Transformation Engineering Co., Ltd..

Minsheng Du He main research directions are large-capacity power electronics, new power transmission technologies and the application of intelligent optimization algorithms in power systems. He is a deputy engineer at Gansu Power Transmission and Transformation Engineering Co., Ltd..

Liang Hua He main research directions are the application of MPC in industrial process control, and the optimal scheduling and control strategy of power system. He is a deputy engineer at Gansu Power Transmission and Transformation Engineering Co., Ltd..

Binyuan Shi He main research directions are the stability study of linear time-delay systems, modeling of time-delay systems and control of time-delay systems. He is a deputy engineer at Gansu Power Transmission and Transformation Engineering Co., Ltd..

Dong Lan He main research directions are the combination of PID control and Smith estimator, and smart grid engineering management. He is a deputy engineer at Gansu Power Transmission and Transformation Engineering Co., Ltd..

Sangen Ding He main research directions are the commissioning and safety management of relay protection devices, and the application of relay protection technology in smart grids. He is an engineer at Gansu Power Transmission and Transformation Engineering Co., Ltd..

Binwu Zhang He main research directions are the safety and stability operation technology of power systems, and the operation and maintenance technology and management of power grid substations. He is an engineer at State Grid Wuwei Power Supply Company.